IOP Publishing Journal of Physics D: Applied Physics
J. Phys. D: Appl. Phys. **50** (2017) 484004 (7pp) https://doi.org/10.1088/1361-6463/aa92a5

Generation of surface acoustic waves on doped semiconductor substrates

M Yuan[1], C Hubert[1], S Rauwerdink[1], A Tahraoui[1], B van Someren[2], K Biermann[1] and P V Santos[1]

[1] Paul-Drude-Institut für Festkörperelektronik, Hausvogteiplatz 5-7, 10117 Berlin, Germany
[2] Elf Software B.V., Eikenpage 31, 3061 WS Rotterdam, Netherlands

E-mail: yuan@pdi-berlin.de

Received 18 August 2017, revised 5 October 2017
Accepted for publication 11 October 2017
Published 8 November 2017

Abstract

We report on the electrical generation of surface acoustic waves (SAWs) on doped semiconductor substrates. This is implemented by using interdigital transducers (IDTs) placed on piezoelectric ZnO films sputtered onto evaporated thin metal layers. Two material systems are investigated, namely ZnO/Au/GaAs and ZnO/Ni/InP. The rf-field applied to the transducer is electrically screened by the highly conductive metal film underneath the ZnO film without any extra ohmic losses. As a result, absorption of the rf-field by the mobile carriers in the lossy doped region underneath the IDT is avoided, ensuring efficient SAW generation. We find that the growth temperature of the ZnO film on the metal layer affects its structure and, thus, the efficiency of SAW generation. With this technique, the SAW active layers can be placed close to doped layers, expanding the application range of SAWs in semiconductor devices.

Keywords: surface acoustic waves, ZnO on metal film, doped semiconductor, nonpiezoelectric substrate

(Some figures may appear in colour only in the online journal)

1. Introduction

Surface acoustic waves (SAWs) in the GHz range have favorable properties for the modulation and control of electronic, optical, and magnetic excitation in semiconductors [1]. These waves can be easily generated by applying a radio-frequency field to interdigital transducers (IDTs) deposited on a piezoelectric substrate. Their time dependent fields modulate the material's optical properties and produce a moving potential for the transport of electrons [2–5] as well as excitons [6–10]. The generation and propagation of SAWs on doped regions are normally hindered by the electrical screening of the applied rf-field by free carriers, which prevents the efficient piezoelectric generation using interdigital transducers (IDTs), and by SAW absorption due to the lossy conductivity [11]. Consequently, most of the studies have been carried out using SAWs electrically generated in an undoped region of the sample. In the case of the acoustic transport of electrons, for instance, the doped layers supplying the electrons are either grown on a mesa [2] or removed from the IDT area [4, 5].

Doped layers, however, are ubiquitous in semiconductor electro-optical structures: the compatibility of SAW generation with doped layers is a crucial issue that can considerably improve the flexibility of SAW modulation. A current solution is to place the doped region far away from the sample surface (i.e. at a depth on the order of one SAW wavelength λ_{SAW} [6, 10]). In this case, the coupling strength between the SAW and the system in interest is usually compromised. The approach we investigate in this report uses IDTs fabricated on a stack consisting of a piezoelectric film (e.g. ZnO) on a thin, highly-conductive metal film deposited on the doped substrate. The deposition of ZnO on a metal for the generation of bulk acoustic waves on non-piezoelectric substrates was studied in the 60 s and the 70 s. Bulk acoustic transducers consisting of ZnO sputtered on an Au film were used for the efficient generation of bulk waves in sapphire and fused quartz [12, 13]. The theory of SAW generation using IDTs deposited on a piezoelectric ZnO film on Au was extensively studied [14]. Wagers *et al* [15] applied this process for SAW generation on fused silica. The experimental results presented by them qualitatively agree with

the theory. In particular, the piezoelectric coupling constant K^2 was found to depend on the thickness of the ZnO film and the quality of the substrates were found to affect the generation of SAWs [14, 15]. These studies were all based on undoped semiconducting substrates or insulating substrates.

The combination of ZnO and metal films can also be applied to doped semiconductors. To our knowledge, however, experimental results have so far not been reported for doped substrates with a large concentration of free carriers. In this paper, we study the generation of SAWs using IDTs overlaid with piezoelectric ZnO/metal islands on doped semiconductor substrates. The thin metal film, e.g. Au or Ni, is first evaporated on the doped substrate and subsequently sputter-coated with a piezoelectric ZnO film. SAWs are then generated using IDTs photo-lithographically defined on top of the piezoelectric ZnO islands.

The presence of the metal film between the piezoelectric film and the nearby doped region is crucial for the excitation of SAWs. Since the plasma frequency of metals f_p is much higher than the SAW frequency f_{SAW}, $f_p \gg f_{SAW}$, carriers in the metal can relax quickly from the perturbation by the applied rf-field, which leads to perfect screening. This screening process does not introduce any extra ohmic loss due to the vanishing field build-up inside the metal. Conversely, without the metal film, the applied rf-field will be screened and absorbed by the lossy doped region instead, whose lower plasma frequency results in significant attenuation [11]. Additionally, the metal film concentrates the rf-field in the piezoelectric film, increasing coupling to the acoustic waves [14].

The excited piezoelectric SAW field is also electrically screened by the metal film. Consequently, underneath the IDTs, the SAWs reaching the GaAs close to the metal will be purely mechanical. The $\langle 1\,0\,0\rangle$ propagation direction on GaAs is non-piezoelectric: as a result, a SAW propagating along this direction is not accompanied by electric fields. In other words, in this propagation direction, required for exciton modulation [10], the SAWs traveling outside the ZnO/metal islands will also be purely mechanical. Therefore, the SAW will not be absorbed by the lossy doped layers.

In the next sections, we first describe the structure of the samples and the procedures to fabricate transducers for the generation of SAWs (section 2). We then present the experimental results, namely the ZnO structural properties and the electrical measurement of IDT delay lines (section 3), followed by discussions focused on extracting K^2 from both experiments and simulations (section 4). We conclude in section 5 with a brief summary of the results.

2. Experimental details

2.1. Delay lines on doped GaAs substrates

We fabricated SAW delay lines on heterostructures grown by molecular beam epitaxy (MBE) on n-doped GaAs (0 0 1) substrates represented schematically in figure 1(a). The doping level of the substrate is on the order of 10^{18} cm^{-3}. The MBE layers are undoped and include four GaAs quantum wells (QWs) embedded in AlGaAs barriers with a total thickness of

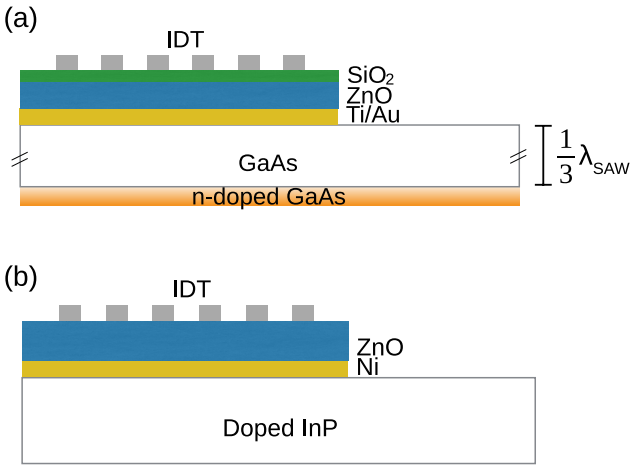

Figure 1. Sample structure for (a) GaAs and (b) InP substrates. IDTs are depositied on ZnO/metal islands.

760 nm—the electro-optical properties of these structures will not be addressed in the present report.

The IDTs were designed for the generation of SAWs with wavelength $\lambda_{SAW} = 2.8$ μm, corresponding to a resonant frequency of $f_{SAW} \sim 1$ GHz. The ratio between the depth of the doped substrate and λ_{SAW} is thus equal to 0.27, considerably smaller than 1. The transmitter-receiver IDT pairs in the SAW delay lines were oriented along either the $\langle 1\,0\,0\rangle$ (non-piezoelectric) direction or the $\langle 1\,1\,0\rangle$ (piezoelectric) direction. The spacing between the transmitter and the receiver is 650 μm.

For the fabrication of the delay lines, Ti/Au islands with a thickness of 10/40 nm were first patterned on the surface by electron-beam evaporation and lift-off. Subsequently, we deposited a 200 nm-thick ZnO layer by sputtering and capped it with 15 nm of SiO_2 for protection. In order to ensure piezoelectricity, the sputtered ZnO films must be textured with the hexagonal c-axis perpendicular to the sample surface [13]. In previous studies (see, e.g. [16, 17]), we found that the piezoelectric properties improve when the ZnO films are sputtered at high temperatures (typically between 300 °C and 350 °C) on silicon substrates. Here, we show that the ZnO sputtering conditions need to be modified for deposition on metals. We will show in section 3 experimental results for samples with the ZnO film sputtered at room temperature (sample GaAs-A) and at 350 °C (sample GaAs-B). The ZnO film was then selectively etched to form islands on which the IDTs for delay lines oriented along $\langle 1\,0\,0\rangle$ or $\langle 1\,1\,0\rangle$ were photo-lithographically defined by electron-beam evaporation and lift-off. The single-finger IDTs for the GaAs samples consist of a stack of Ti/Al/Ti (10 nm/30 nm/10 nm) films. Each IDT consists of $N = 150$ pairs of electrode fingers in the conventional single-finger form with alternating polarities. Note that the SAWs generated within the ZnO film penetrates the Au film and reaches the doped substrate. The piezoelectrical component of the SAW field is absent for the $\langle 1\,0\,0\rangle$ propagation direction.

2.2. Delay lines on doped InP substrates

We also investigated SAW generation on doped (0 0 1) InP substrates using the IDT structure displayed in figure 1(b).

The doping level of the whole substrate is 4.7×10^{18} cm^{-3}. The substrates were in this case initially coated with a 150 nm-thick Ni layer and then sputtered with 50 nm of SiO_2 and the piezoelectric ZnO film. Different ZnO film thicknesses and sputtering temperatures were investigated in order to determine the appropriate conditions to obtain good piezoelectric properties. We will present here results for structures with a ZnO layer thickness of 500 nm sputtered at room temperature (sample InP-A) and for another sample with a 250 nm-thick ZnO film sputtered at 300 °C (sample InP-B). Delay lines for an acoustic wavelength $\lambda_{SAW} = 5.6$ μm and oriented along the [1 $\bar{1}$ 0] surface direction of the (0 0 1) InP substrate were then fabricated on the ZnO films using optical lithography and lift-off. The IDTs in the delay line are of the single-finger type with an aperture and length of 120 μm and 1960 μm, respectively.

2.3. rf-measurements

The electrical properties of the delay lines were studied by performing S-parameter (scattering matrix) measurement in a probe station at room temperature. The rf signal was applied between IDT fingers of different polarities. The underlying metal ground plane was left floating. We also monitored the dc resistance between the signal contacts and the ground contacts of the IDTs to detect any current leakage between the IDT fingers and the metal layer underneath.

3. Results

3.1. ZnO structural properties

In sample GaAs-A SAW resonances were detected in all 32 IDT pairs fabricated on a wafer. In sample GaAs-B, in contrast, we could not detect any SAW resonance. The dc-resistance measurements between the IDT pads yield values smaller than 100 Ω for this sample, thus indicating that the IDT contacts are short-circuited.

The difference in sample processing between sample GaAs-A and GaAs-B lies in the growth temperature of the ZnO layer, with sample GaAs-A sputtered at room temperature and sample GaAs-B at 350 °C. Micrographs from the sample surfaces obtained with atomic force microscopy (AFM) shown in figure 2 confirm that the surfaces of the two samples have qualitatively different characteristics. In the case of sample GaAs-A, the layer is smooth and the grain size is typical for ZnO film with the hexagonal *c*-axis oriented perpendicularly to the surface. In sample GaAs-B, however, there is a distribution of pits with a diameter of a few microns and a depth of over 30 nm, corresponding to the thickness of the Au layer. High growth temperature (350 °C) creates pits in the Au surface, which we have confirmed by depositing the Ti/Au layer on a GaAs substrate and subsequently heating up to 350° without sputtering ZnO. The rough surface short-circuits the IDTs. Room temperature growth, in contrast, provides a smooth surface without pits, which enables efficient SAW generation.

Qualitatively similar results were obtained for ZnO films deposited on Ni layers on InP, as demonstrated by optical

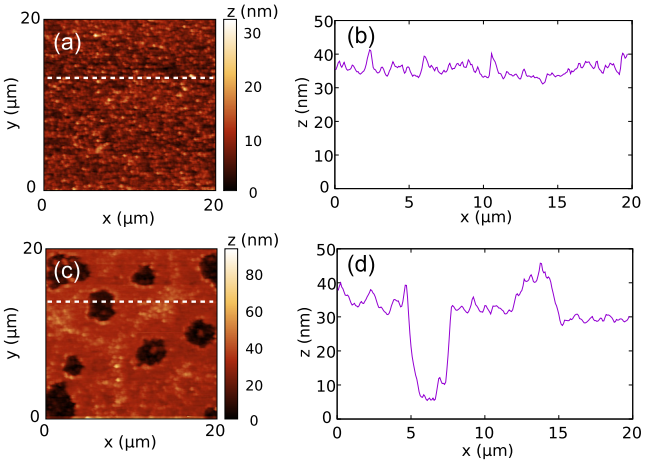

Figure 2. AFM images of sample surface. (a) GaAs-A sputtered at RT. (b) Cross-section of (a) along the dashed line. (c) GaAs-B sputtered at 350 °C showing micron-sized pits on the sample surface. (d) Cross section of (c) along the dashed line.

micrographs of figure 3. While films sputtered at high temperature (300 °C, figure 3(c)) exhibit a high density of pits, as well as low transducer fabrication yield, the ones deposited at room temperature (figure 3(a)) are smooth and with good piezoelectric properties. We also found the density of pits in films deposited at high temperatures can be reduced by decreasing the ZnO thickness. This result indicates that the pits are probably associated with metal peeling due to the difference in the thermal expansion coefficient between the metal and the ZnO film. In fact, Ni and Au have thermal expansion coefficients of $\sim 14 \times 10^{-6}$ K^{-1}, which are larger than the ones for ZnO ($3–4 \times 10^{-6}$ K^{-1}), GaAs (6.86×10^{-6} K^{-1}), and InP (4.75×10^{-6} K^{-1}) crystals.

3.2. Delay line properties

3.2.1. Delay lines on GaAs. Examples of s-parameter measurements for GaAs-A are shown in figure 4. The reflection (S_{11}) and transmission coefficients (S_{12}) for a delay line along the non-piezoelectric ⟨1 0 0⟩ direction are plotted in the upper panels. The corresponding coefficients for a delay line along the piezoelectric ⟨1 1 0⟩ direction are shown in the lower panels. The SAW resonance occurs at 0.953 and 0.983 GHz for ⟨1 0 0⟩ and ⟨110⟩, respectively. For ⟨1 0 0⟩, the S_{11} dip is 0.25 dB and the transmission peak reaches −37 dB. The resonance dip in the reflection coefficient is reduced to about 0.1 dB and the level of the transmission peak is about −45 dB for the ⟨1 1 0⟩ direction. The lower acoustic transmission and generation efficiency for the delay lines along ⟨1 1 0⟩ is attributed to the fact that SAWs along this direction are accompanied by a piezoelectric potential. The latter interacts strongly with free carriers along the propagation path, thus leading to SAW damping.

3.2.2. Delay lines on InP. Figures 3(b) and (d) compare the electrical reflection and transmission coefficients for delay lines ⟨1 1 0⟩ using ZnO sputtered at room temperature (sample InP-A) and at 300° (InP-B). Acoustic resonances at about 460 MHz have been observed in both cases: the acousto-electric

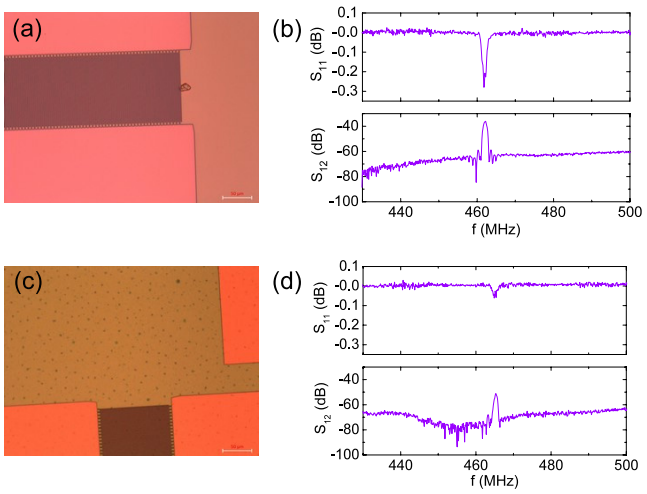

Figure 3. (a) Optical micrographs and (b) S-parameters for a delay line on a ZnO/SiO_2/Ni island on doped InP. The 500 nm-thick piezoelectric ZnO was sputtered at room temperature (sample InP-A). (c)–(d) Corresponding data for a delay line with a 250 nm-thick ZnO layer sputtered at 300 °C (sample InP-B). The delay lines each have two IDTs for an acoustic wavelength $\lambda_{SAW} = 5.6$ μm. In both cases, the Ni and SiO_2 films are 150 and 50 nm thick, respectively.

properties are, however, much better for ZnO deposition at room temperature, which exhibits an S_{12} peak of −37 dB, 16 dB higher than its high-temperature counterpart. As in the case of GaAs, the acousto-electric performance correlates with the structural properties of the films.

4. Discussions

4.1. Equivalent circuit and K^2

In this section we extract the piezoelectric constant K^2 from the measured S_{12}. We define the SAW wavelength λ_{SAW}, the IDT beam width W, the distance between the metal layer, e. g. Au and the surface d, and the number of electrode pairs N. The equivalent circuit (Mason model) of a transmitting IDT is illustrated in figure 5. A source with impedance $R_g = 50\ \Omega$ and voltage V is driving the IDT, which has a complex admittance $Y(f) = G_a(f) + jB_a(f)$, and a capacitance of C_T. Here, G_a and B_a represent the acoustic conductance and the acoustic susceptance, respectively. The insertion loss is defined as the power delivered to the SAW normalized to the applied rf power. For a single bidirectional IDT modeled in figure 5, the insertion loss in dB can be derived as [18]

$$\mathrm{IL}_s = -10\log_{10}\frac{2G_aR_g}{(1+G_aR_g)^2 + [R_g(2\pi fC_T + B_a)]^2}. \quad (1)$$

The transmitter-receiver IDT pair is a reciprocal network. The delay region is assumed to be lossless, therefore the pair insertion loss in dB will be twice the single insertion loss in dB:

$$\mathrm{IL}_p = 2 \times \mathrm{IL}_s. \quad (2)$$

The pair insertion loss can be related to S_{21} (in dB) by

$$S_{21} = -\mathrm{IL}_p. \quad (3)$$

For reciprocal networks $S_{12} = S_{21}$. In our case, it can be shown that the product $G_aR_g \ll 1$. In addition, at resonant frequency f_0, $B_a = 0$, in which case equation (1) can be simplified as

$$\mathrm{IL}_s = -10\log_{10}\frac{2G_aR_g}{1+(R_g2\pi fC_T)^2}. \quad (4)$$

For a single IDT with a nearby ground plane (in our case, the Au or Ni films) whose distance from the surface $d \ll \lambda$, K^2 can be related to the conductance $G(f)$ evaluated at the resonant frequency f_0 via the following equation [18]:

$$G(f_0) = 2 \times N^2\left|\frac{1}{\sqrt{2}}jK^2\right|^2 Y_0. \quad (5)$$

Here, $j = \sqrt{-1}$ and Y_0 is the characteristic admittance of the SAW beam with beam width W and wavelength λ. One should distinguish between $Y(f)$ and Y_0. The former is the transduction admittance relating the transduced SAW power flow with the voltage on the IDT, while the latter characterizes the transmission line model of the SAW beam alone, regardless of the IDT. Since the generated piezoelectric potential is much smaller than the voltage across the IDT due to small K^2, for one pair of electrod ($N = 1$), $Y \ll Y_0$. As can be seen in equation (5), the difference between them lies in K^2 and can be compensated by using large N. In the case of $d \ll \lambda$ the following equation relating Y_0 to the piezoelectric coupling constant K^2 can be derived [18]:

$$K^2\frac{Y_0}{W} = \frac{\epsilon_p^z v_0}{d}. \quad (6)$$

Here, ϵ_p^z and v_0 are the permittivity in z direction and the surface wave velocity in the piezoelectric material, respectively. The IDT capacitance is the sum of the inter-finger capacitance and the parallel plate capacitor between the electrodes and the ground plane, the area of the latter being much bigger than the former:

$$C_T = N(\epsilon_0 + \epsilon_p^x)W + \frac{N}{8}\epsilon_p^z W\frac{\lambda}{d}, \quad (7)$$

where ϵ_0 is the vacuum permittivity and ϵ_p^x the permittivity in x direction. Combining equations (4)–(6) we can obtain the following approximation for K^2:

$$K^2 = |S_{12}(f_0)|\frac{1+(R_g2\pi fC_T)^2}{2N^2\epsilon_p v_0\frac{W}{d}R_g}. \quad (8)$$

Note that for a delay line with two IDTs, $|S_{12}|$ is equal to the ratio between their respective voltages.

From equation (5) it is obvious that the conductance is proportional to $(K^2N)^2$. This is violated if internal reflection, which is a second-order effect becomes significant. To evaluate the impact of this effect we can turn to the expression for the frequency dependence of S_{12} around f_0 [18]:

$$|S_{12}| \propto \left|\frac{\sin N\pi\frac{\Delta f}{f_0}}{N\pi\frac{\Delta f}{f_0}}\right|. \quad (9)$$

The $\frac{\sin x}{x}$ profile arises from the frequency response of the IDT, which is the Fourier transform of its impulse response. The first

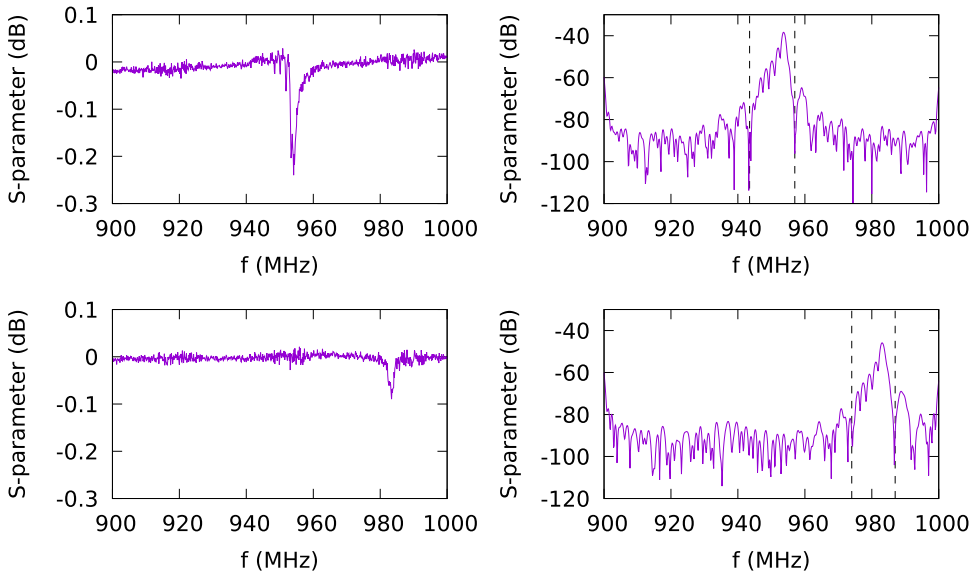

Figure 4. S-parameters for IDTs along $\langle 1\,0\,0\rangle$ (upper panel) and $\langle 1\,1\,0\rangle$ (lower panel), sample GaAs-A. S_{11} and S_{12} are plotted in the left/right panels. The SAW generation efficiency along $\langle 1\,0\,0\rangle$ is higher than along $\langle 1\,1\,0\rangle$.

local minimum of $|S_{12}|$ occurs at a frequency shift Δf satisfying $N\pi\frac{\Delta f}{f_0} = \pi$. For $N = 150$, $f_0 \sim 1$ GHz, $\Delta f \sim 6.7$ MHz. From figure 4, we estimate $\Delta f \sim 6.5$ MHz for both $\langle 1\,0\,0\rangle$ and $\langle 1\,1\,0\rangle$ (see dashed lines, showing $2\Delta f$), in good agreement with the expected value, which indicates that internal reflection can be ignored and $N = 150$ is a good representation of the effective number of electrode pairs. For GaAs-A, $W = 100$ μm, $d = 40$ nm, $\lambda = \lambda_{\mathrm{SAW}} = 2.8$ μm, $\epsilon_p^z = 1.12$ pF cm^{-1}, $\epsilon_p^x = 0.9$ pF cm^{-1} and $v_0 = 2810$ m s^{-1}. We extract $K^2 = 0.01\%$ for $\langle 1\,0\,0\rangle$ and $K^2 = 0.004\%$ for $\langle 1\,1\,0\rangle$.

4.2. Simulation

The spatial distribution of the acoustic fields and the electrical properties of the delay lines were also calculated using a two-dimensional (2D) model for the SAW delay line. We use for that purpose the finite element approach described in [19, 20]. The 2D numerical simulations determines the SAW field in a x-z cross-section of the structure in figure 1, where $x \| \langle 1\,0\,0\rangle, \langle 1\,1\,0\rangle$ corresponds to the SAW propagation direction and $z \| [0\,0\,1]$ is the surface normal. The delay lines consist of two IDTs with a length of $50\lambda_{\mathrm{SAW}}$, the spacing between them being $20\lambda_{\mathrm{SAW}}$. The 40 nm thick Al fingers have each a width of $\lambda_{\mathrm{SAW}}/4$, which is also the spacing between neighboring fingers. Undoped GaAs substrate is used for simplicity. The calculation domain was surrounded by perfectly matched layers (PMLs) with a thickness of $5\lambda_{\mathrm{SAW}}$ to avoid the effect of acoustic reflections at the border areas.

In order to determine the S-parameters, an rf-voltage with a frequency f is applied to the left IDT of the delay line (IDT_1, used as a SAW emitter). We then solve the elastic and piezoelectric equations to determine the spatial distribution of the strain and piezoelectric fields across the structure. The latter is then used to calculate the rf signal detected by the second IDT (IDT_2, used as receiver).

The result of the simulation is shown in figure 6. In figure 6(a) a cross-section of the sample layout is shown with the color code corresponding to the amplitude of mechanical displacement of the SAW, $|u|$. Outside of the transmitter the SAW can propagate in both direction. The wave that travels towards the receiver contributes to the transmission coefficient, while the one that travels in the opposite direction does not. The S-parameters of the two-port network is calculated repeatedly for a range of frequency between 0.9 and 1 GHz, stepping every 0.001 GHz. The result is plotted in figures 6(b)–(e). For $\langle 1\,0\,0\rangle$ the resonance occurs at 0.946 GHz, with a dip of 1.58 dB in S_{11} (figure 6(b)) and a peak of -21.8 dB in S_{12} (figure 6(c)). For $\langle 1\,1\,0\rangle$ S_{11} shows a resonance dip of 2 dB at 0.974 GHz (figure 6(d)) and the peak height in S_{12} is -19.6 dB (figure 6(e)). The simulated Δf is 19 MHz, which agrees with the first-order expectation. The corresponding K^2 is 0.434% for $\langle 1\,0\,0\rangle$ and 0.558% for $\langle 1\,1\,0\rangle$.

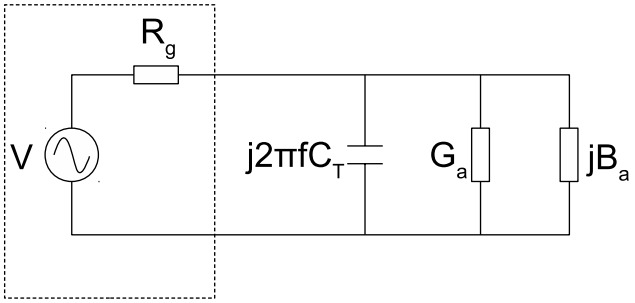

Figure 5. Circuit model of a transmitting IDT following the model discussed in [18].

Compared with the simulated results, S_{12} peaks from sample GaAs-A are much smaller. It suggests that the piezoelectric quality of our sputtered ZnO layer is different from the crystalline ZnO values [21, 22] used in the simulation. Nevertheless, the crystalline ZnO values yield relatively accurate resonant frequencies. (We have also performed another simulation using reported sputtered ZnO coefficients [23]. The corresponding simulated resonant frequencies do not agree with the experimental values, about 30 MHz too low.) In addition, the substrate used in the simulation is undoped. In

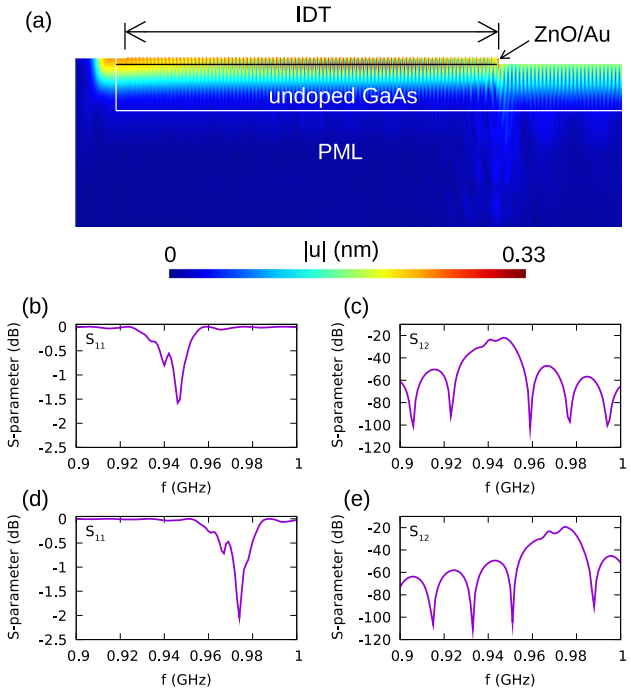

Figure 6. Simulated result for IDTs on ZnO/Au islands with $N = 50$ pairs of electrodes for each IDT. (a) Profiles of SAW field displacement amplitude. Only the emitting IDT and part of the PML used to suppress boundary reflections are shown. For better visualization the axes are scaled to a height-to-width ratio of 8. (b)–(e) S-parameter for IDTs along $\langle 1\,0\,0 \rangle$ (b), (c) and $\langle 1\,1\,0 \rangle$ (d), (e).

reality, the electrical screening from the thin metal films may not be perfect and the remnant of the electrical fields accompanying the SAWs can interact with the doped substrates, resulting in SAW attenuation.

5. Conclusion

We have demonstrated that SAWs can be generated in the vicinity of doped layers in semiconductor substrates by IDTs deposited on ZnO/metal islands. With this technique, the active layers can be placed close to the doped substrate, significantly benefiting the control of excitons and electrons in QW structures. This technique can be extended to other applications of SAWs in semiconductor electro-optical devices. Alternative piezoelectric films, such as $LiNO_3$ [24] and AlN [25] can also be used to generate SAWs. The technique presented here enables the generation of SAWs in doped semiconductor structures, opening a new window for hybrid acoustic devices.

Acknowledgment

We acknowledge support from the German Deutsche Forschungsgemeinschaft: 9173.

ORCID iDs

M Yuan https://orcid.org/0000-0002-7627-3916

References

[1] de Lima M M Jr and Santos P V 2005 Modulation of photonic structures by surface acoustic waves *Rep. Prog. Phys.* **68** 1639

[2] Shilton J M, Talyanskii V I, Pepper M, Ritchie D A, Frost J E F, Ford C J B, Smith C G and Jones G A C 1996 High-frequency single-electron transport in a quasi-one-dimensional GaAs channel induced by surface acoustic waves *J. Phys.: Condens. Matter* **8** L531

[3] McNeil R P G, Kataoka M, Ford C J B, Barnes C H W, Anderson D, Jones G A C, Farrer I and Ritchie D A 2011 On-demand single-electron transfer between distant quantum dots *Nature* **477** 439–42

[4] Hermelin S, Takada S, Yamamoto M, Tarucha S, Wieck A D, Saminadayar L, Bauerle C and Meunier T 2011 Electrons surfing on a sound wave as a platform for quantum optics with flying electrons *Nature* **477** 435–8

[5] Hermelin S, Takada S, Yamamoto M, Tarucha S, Wieck A D, Saminadayar L, Bäuerle C and Meunier T 2013 Fast and efficient single electron transfer between distant quantum dots *J. Appl. Phys.* **113** 136508

[6] Rudolph J, Hey R and Santos P V 2007 Long-range exciton transport by dynamic strain fields in a GaAs quantum well *Phys. Rev. Lett.* **99** 047602

[7] Rudolph J, Hey R and Santos P V 2007 Exciton transport by surface acoustic waves *Superlattices Microstruct.* **41** 293–6

[8] Lazić S, Santos P V and Hey R 2010 Exciton transport by moving strain dots in GaAs quantum wells *Physica* E **42** 2640–3

[9] Lazić S S, Violante A, Cohen K, Hey R, Rapaport R and Santos P V 2014 Scalable interconnections for remote indirect exciton systems based on acoustic transport *Phys. Rev.* B **89** 085313

[10] Violante A, Cohen K, Lazić S, Hey R, Rapaport R and Santos P V 2014 Dynamics of indirect exciton transport by moving acoustic fields *New J. Phys.* **16** 033035

[11] Wixforth A, Scriba J, Wassermeier M, Kotthaus J P, Weimann G and Schlapp W 1989 Surface acoustic waves on GaAs/$Al_xGa_{1-x}As$ heterostructures *Phys. Rev.* B **40** 7874

[12] Foster N F and Rozgonyi G A 1966 Zinc oxide film transducers *Appl. Phys. Lett.* **8** 221

[13] Foster N F 1969 Crystallographic orientation of zinc oxide films deposited by triode sputtering *J. Vac. Sci. Technol.* **6** 111

[14] Kino G S and Wagers R S 1973 Theory of interdigital couplers on nonpiezoelectric substrata *J. Appl. Phys.* **44** 1480–8

[15] Wagers R, Kino G, Galle P and Winslow D 1972 ZnO acoustic transducers utilizing crystalline gold substrate *Ultrasonics Symposium* p 194

[16] Batista P D, Drescher B, Seidel W, Rudolph J, Jiao S and Santos P V 2008 ZnO/SiO_2 microcavity modulator on silicon *Appl. Phys. Lett.* **92** 133502

[17] Büyükköse S, Vratzov B, van der Veen J, Santos P V and van der Wiel W G 2013 Ultrahigh-frequency surface acoustic wave generation for acoustic charge transport in silicon *Appl. Phys. Lett.* **102** 013112

[18] Datta S 1986 *Surface Acoustic Wave Devices* (London: Prentice Hall)

[19] Geuzaine C and Remacle J-F 2009 Gmsh: a three-dimensional finite element mesh generator with built-in pre- and post-processing facilities *Int. J. Numer. Methods Eng.* **79** 1309

[20] Dular P, Geuzaine C, Henrotte F and Legros W 1998 A general environment for the treatment of discrete problems and its application to the finite element method *IEEE Trans. Magn.* **34** 3395

[21] Madelung O ed 1983 *Landolt-Börnstein Tables, New Series, Group III: Solid State Physics, Low Frequency Properties of Dielectric Crystals: Second and Higher Order Elastic Constants* vol 29a (Berlin: Springer) (https://doi.org/10.1007/b44185)

[22] Royer D and Dieulesaint E 2000 *Elastic Waves in Solids I* (Berlin: Springer)

[23] Gualtieri J G, Kosinski J A and Ballato A 1994 Piezoelectric materials for acoustic wave applications *IEEE Trans. Ultrason. Ferroelectr. Frequation Control* **41** 53–9

[24] Baumann R C, Rost T A and Rabson T A 1990 Deposition and physical characterization of thin films of lithium niobate on silicon substrates *J. Appl. Phys.* **68** 2989–91

[25] Caliendo C and Imperatori P 2004 Structural, optical, and acoustic characterization of high-quality aln thick films sputtered on Al_2O_3 (0 0 0 1) at low temperature for GHz-band electroacoustic devices applications *J. Appl. Phys.* **96** 2610